

Article

Microstructural Analysis and Compressive Strength of Fly Ash and Petroleum Sludge Ash Geopolymer Mortar under High Temperatures

Mubarak Usman Kankia ^{1,2}, Lavania Baloo ^{1,*} , Nasiru Danlami ³, Noor Amila Zawawi ¹ , Abosede Bello ² and Sadiq Ibrahim Muhammad ²

- ¹ Civil and Environmental Engineering Department, Universiti Teknologi PETRONAS, Seri Iskandar 32610, Malaysia; mubarak_18001828@utp.edu.my (M.U.K.); amilawa@utp.edu.my (N.A.Z.)
² Tertiary Education Trust Fund (TETFUND), Maitama District, Abuja 900271, Nigeria; belloaa@tetfund.gov.ng (A.B.); ibrahimms@tetfund.gov.ng (S.I.M.)
³ Civil Engineering Department, Bayero University, PMB 3011, Kano 700006, Nigeria; nasiru_g03164@utp.edu.my
* Correspondence: lavania.baloo@utp.edu.my; Tel.: +60-135-001-755

Abstract: The development of sustainable building materials and construction to decrease environmental pollution in both production and operational stages of the materials' life cycle is appealing to great interest in the construction industries worldwide. This study evaluated the negative effect of temperature up to 1000 °C on the compressive strength and microstructure of fly ash and petroleum sludge ash (PSA) geopolymer mortar. A sodium silicate and sodium hydroxide mixture is used as an activator. The synthesized mortar was investigated using X-ray Diffraction (XRD), Fourier Transformation Infrared Spectroscopy (FTIR), Mercury Intrusion Porosimetry (MIP), and Field Emission Scanning Electron Microscopy (FESEM). As the temperature increased, the compressive strength of the geopolymer mortar decreased. The strength degradation is due to the damage to microstructure because of the temperature-induced dehydroxylation, dehydration thermal incompatibility between geopolymer aggregate and paste of geopolymer mortar at high temperatures. With an increase in temperature, the cumulative pore volume increased. The FESEM image showed the decomposition of the geopolymer matrix started at a temperature of 600 °C. Incorporating PSA in geopolymer mortar could result in an eco-friendly and sustainable environment that may reduce the problems associated with sludge disposal.

Keywords: petroleum sludge ash; compressive strength; fly ash; geopolymer mortar; elevated temperatures; microstructural analyses



check for updates

Citation: Usman Kankia, M.; Baloo, L.; Danlami, N.; Zawawi, N.A.; Bello, A.; Muhammad, S.I. Microstructural Analysis and Compressive Strength of Fly Ash and Petroleum Sludge Ash Geopolymer Mortar under High Temperatures. *Sustainability* **2023**, *15*, 9846. <https://doi.org/10.3390/su15129846>

Academic Editor: John Vakros

Received: 27 April 2022

Accepted: 26 September 2022

Published: 20 June 2023



Copyright: © 2023 by the authors. Licensee MDPI, Basel, Switzerland. This article is an open access article distributed under the terms and conditions of the Creative Commons Attribution (CC BY) license (<https://creativecommons.org/licenses/by/4.0/>).

1. Introduction

Over the past decades, ordinary Portland cement (OPC) has become one of the manufactured materials for construction worldwide because of its availability, versatility and highly reliable performance and the comparatively low cost of OPC raw materials as well as processing technology [1–3]. Unfortunately, the production of OPC requires high energy needed for limestone calcination. Furthermore, deleterious gases like nitrogen oxide, carbon dioxide, and SO₃ are discharged into the surrounding environment, resulting in global warming as well as acid rain. In addition, to produce every ton of cement, the industry contributes about 0.7 to 1.1 tons of CO₂ and about 4 GJ of energy is consumed [4]. Additionally, OPC has satisfactory strength to resist fire adverse effects in normal cases. OPC is used as a fire-resistant cover to the reinforcement but at high temperatures, it shows physical and chemical changes along with a decrease in mechanical properties. Calcium hydroxide (CaOH₂) is obtained from the product of the hydration reaction of OPC which gives the strength to decompose at about 400 °C to water and calcium oxide (CaO) [5].

At a temperature higher than 400 °C, total strength loss occurs due to the dehydration and dissociation of CaOH_2 and rehydration of CaO . Calcium–silicate–hydrate gel (CSH), a strength-giving compound, further decomposes above 600 °C and at about 800 °C the concrete usually crumbled [6,7]. Additionally, the feldspar and other minerals of the cement paste melt above 1150 °C and turn into a glass phase. Khoury [8] stated three mechanisms that affect the strength of Portland cement-based materials at higher temperatures including thermal incompatibility, effects of phase transformation, and pore pressure. However, since the general acceptance of ‘sustainability’ as a vital criterion for the evaluation of building materials by the engineering community, OPC is becoming unsustainable [9]. Therefore, it is of paramount importance to seek new materials that have improved properties at higher temperatures. At this point, among the study of binder alternatives to cement, geopolymers are one of the promising ideal products as new cementing materials through the utilization of waste materials which have the potential to be important components in environmentally sustainable construction.

Agricultural and industrial wastes are rapidly increasing because of the fast growth of urbanization and industrialization which could be utilized as the potential precursor/pozzolanic materials in the building industries [10]. Recently, ash is an amorphous material containing CaO , Al_2O_3 , and SiO_2 that has been researched which could either partially or fully replace cement. The enormous number of wastes such as fly ash, bottom ash, wood ash, palm oil fuel ash, ground granulated blast furnace slag ash, silica fume, rice husk ash, petroleum sludge ash, and fluidized bed combustion ash pose great threats to human health and the general environment [11,12]. In southeast Asia, the coal utilization in power plants and crude oil in refineries result in the high production of fly ash and petroleum sludge. In Malaysia, both petroleum sludge and fly ash were classified under scheduled wastes by the department of environment (DOE) [13]. The DOE banned the direct disposal of these wastes into landfills because of the concentrated heavy metals [14]. These waste materials could be immobilized in the network of three-dimensional polymer chain structures.

Geopolymer is a new environmentally friendly substitute cementitious material that could even be better than OPC [15–17]. The geopolymer can be made by mixing pozzolanic materials (fly ash, ground granulated blast furnace slag ash, rice husk ash) rich in aluminosilicate mineral (Si-Al) with alkaline solutions such as alkali silicate (sodium silicate solution (Na_2SiO_3), or potassium silicate solution (K_2SiO_3)) and alkali hydroxide (sodium hydroxide (NaOH) or potassium hydroxide (KOH)); reacting together producing an inorganic polymerization process resulting in a strong and durable three-dimensional polymer chain structure of Si-O-Al-O bonds that are semicrystalline or amorphous. After OPC and lime, geopolymer is also recognized as the third generation of cement [13]. The type and concentration of alkaline solution play a vital role in geopolymerization development. NaOH solution has higher solubility of Al^{3+} and Si^{4+} ions compared to KOH solution, hence affecting the compressive strength as well as geopolymer structures [18]. During the NaOH solution preparation, a large amount of heat is emitted, hence before adding the alkaline solution to the dry mix, it is a good idea to get it to room temperature. Geopolymer displays similar durability characteristics and mechanical properties as that of OPC, but it has lower energy consumption with lesser emission of greenhouse gas during its production [19]. The synthesis of geopolymers can be roughly divided into two phases: dissolution-hydrolysis and hydrolysis-polycondensation, both of which can happen at the same time. Following the emission of silicate and aluminate monomers, melting species form which cross-link to form oligomers, resulting in sodium silico-aluminate [20]. The production of gel, as well as setting and hardening, occurs in the following phase, which is linked to polycondensation and the formation of three-dimensional aluminosilicate networks. The Si/Al ratio remains constant during the geopolymerization process, increasing with time. Fly ash-based geopolymers have a low $\text{SiO}_2/\text{Al}_2\text{O}_3$ ratio, which results in high initial strength development. Geopolymers with less content of Si make it likely that more $\text{Al}(\text{OH})_4^{-4}$ species are present for condensation at early stages [15]. Furthermore,

because the Al components dissolve more quickly than the silicon components, the rate of condensation between aluminate and silicate species is faster than the rate of condensation between simply silicate species, resulting in a high initial compressive strength.

Because of fires or other causes, geopolymer mortar and concrete are occasionally subjected to high temperatures. As a result, changes in microstructural properties result in the loss of their strength, and durability is induced [21]. Consequently, exposing geopolymers to high temperatures may cause functional and aesthetic deteriorations to the buildings. Generally, aesthetic damages are easy to repair, while functional impairments can require either partial or total repair, depending upon the magnitude of the damages. Subjecting geopolymer to high temperatures undergoes several transformations and reactions, causing a progressive breakdown of the gel structure and resulting in a loss in its load-bearing capacity, decreased durability, increased tendency of drying shrinkage, and structural cracking. Therefore, studying the temperature effects on the properties of geopolymer mortar/concrete (such as physical and mechanical properties) is of paramount importance [22]. These effects also depend on the type of precursor materials, aggregates raw materials, and the ratio of binder to alkali play significant roles in the production of good geopolymer materials that could withstand the effects of elevated temperature and other environmental conditions. Studies on blended fly ash and slag geopolymers revealed that when exposed to high temperatures, geopolymers performed well in terms of durability (fire resistance, sodium sulfate attack), strength, and thermal shrinkage [23–25].

In this study, the geopolymer mortar compressive strength was measured. In addition, the microstructure (X-ray Diffraction (XRD), Fourier Transformation Infrared Spectroscopy (FTIR), Mercury Intrusion Porosimetry (MIP), and Field Emission Scanning Electron Microscopy (FESEM)) of the fractured surfaces of the geopolymer mortar was investigated.

2. Materials and Methods

2.1. Experiment Materials

A refinery in Malaysia accumulated black, sticky, and semi-solid petroleum sludge. Department of Environment, Malaysia (2010 guidelines) classified petroleum sludge as scheduled waste (SW314). PSA (petroleum sludge ash) was made by burning the sludge and then milling it in a milling machine before sieving it through a 45-micrometer sieve size [26]. The Manjung coal power station in Malaysia provided fly ash (FA) with a high calcium content. The main aluminosilicate source material was FA. The chemical composition of PSA and FA was determined by XRF and is shown in Table 1. The PSA has a total percentage of Al_2O_3 , Fe_2O_3 , and SiO_2 of 70.80 percent, with a loss on ignition (LOI) of 0.09 percent and calcium oxide of 9.26 percent, while the FA has a total percentage of Fe_2O_3 , Al_2O_3 , and SiO_2 of 74%, and so meets the ASTM C618-15 specification [27]. The FESEM was used to determine the morphology of FA and PSA, as shown in Figure 1. The micrograph of PSA (Figure 1a) indicates that the PSA has angular grains whereas the morphology of the FA (Figure 1b) showed spherical particles, allowing them to blend in the mixtures. From a local supplier, the NaOH (NH, purity 99%) and liquid Na_2SiO_3 (NS) with Na_2O 14.37 wt %, SiO_2 29.54 wt%, and H_2O 56.09 wt% were obtained. Sand with 2.52 fineness modulus complying with ASTM C33/C33M—13 was used to make the geopolymer mortar [28]. Figure 2 depicts the PSA XRD pattern. Albite, maghemite, calcite, and cristobalite were the most abundant minerals found.

Table 1. PSA and FA chemical compositions (percent).

	Al_2O_3	Fe_2O_3	SiO_2	P_2O_5	CaO	MgO	TiO_2	SO_3	K_2O	Others	LOI	Blaine Fineness (m^2/kg)	Specific Gravity
PSA	10.00	45.90	14.90	1.75	9.26	2.41	0.41	11.5	1.08	2.70	0.09	117	2.35
FA	17.40	20.20	36.40	1.27	14.5	2.40	1.59	2.01	2.31	1.64	0.28	384	2.68

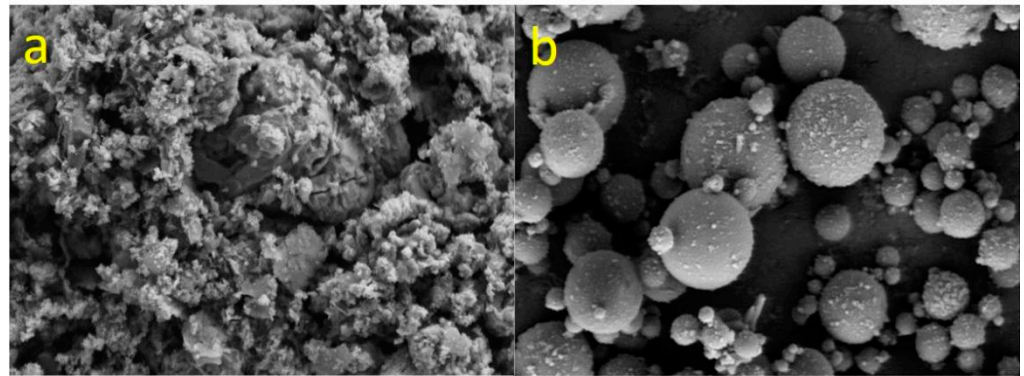


Figure 1. (a) PSA (b) FA FESEM image.

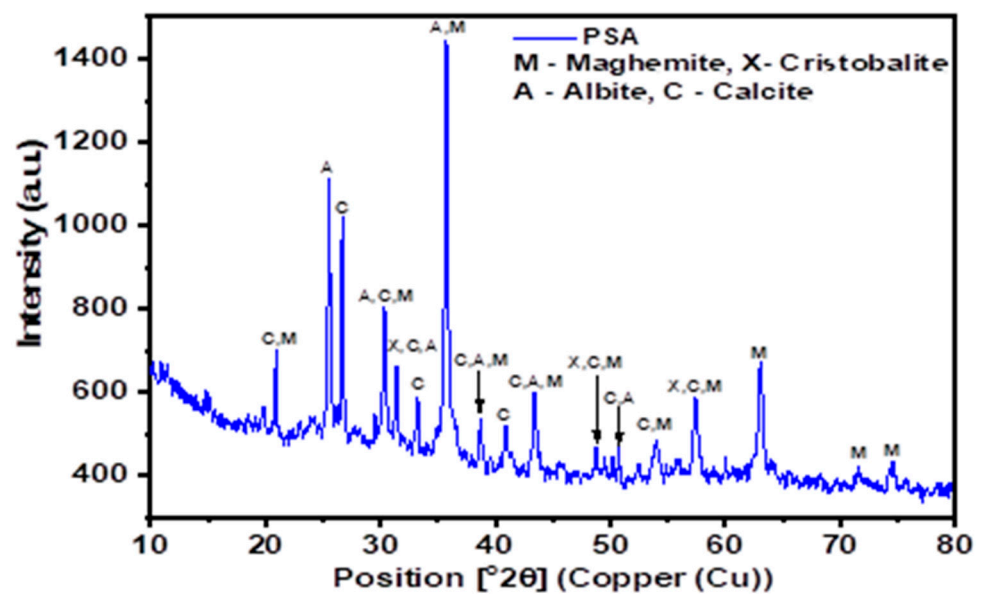


Figure 2. XRD of PSA.

2.2. Preparation of Specimens

The proportions of geopolymer mortar are shown in Table 2. Geopolymer mortar samples were made with a 0.5 alkaline solution to binder ratio, a 2 NS to NH ratio, and a NaOH molarity of 12. In addition, a 1:2 binder-to-sand ratio was employed [29]. The pellets of NH were dissolved in the needed amount of water to make NaOH solution the day before the mortar specimens were made and then allowed to cool to room temperature. The activation solution was made by mixing the requisite amounts of NS and NH solutions homogeneously in a beaker [30]. PSA, FA, and fine aggregates were measured and thoroughly mixed for about two minutes in a Hobart mixer. Furthermore, the mixture was cast into a 50-mm cubic mold. The molds were filled and compacted carefully using a vibrating table for about 30 s. After 1 day, the hardened geopolymer mortar specimens were demolded. The mortar samples were oven cured for 20 h at a temperature of 60 °C [31]. After that, the specimens were maintained in the laboratory at a temperature of 20 ± 2 °C and relative humidity of 60% until the testing day (28th day). The specimens were then placed in an electrical muffle furnace and heated to 200 °C, 400 °C, 600 °C, 800 °C, and 1000 °C. The process of heating the specimen shown in Figure 3, was done according to Payakaniti P. et. al. [32]. 5 °C/min heating rate was used until the temperature targeted was reached. This rate of heating is in line with the standard recommendation of RILEM 129-MHT [33]. The geopolymer mortar specimens were left in the furnace for 60 min at the target temperature. The muffle furnace was turned off once the time had passed [34]. The

mortar specimens were then allowed to cool to laboratory temperature in the furnace. The calcination period for the geopolymer mortar was set to reduce the temperature differential between the inner core and outside surfaces of the mortar samples and to achieve an inner core temperature that was closer to the required temperature.

Table 2. Geopolymer mortar mix proportion.

Sand (kg/m ³)	Alkaline Solution (kg/m ³)	PSA (%)	Fly Ash (kg/m ³)	PSA Content (kg/m ³)
1314.29	328.57	10	591.43	65.71

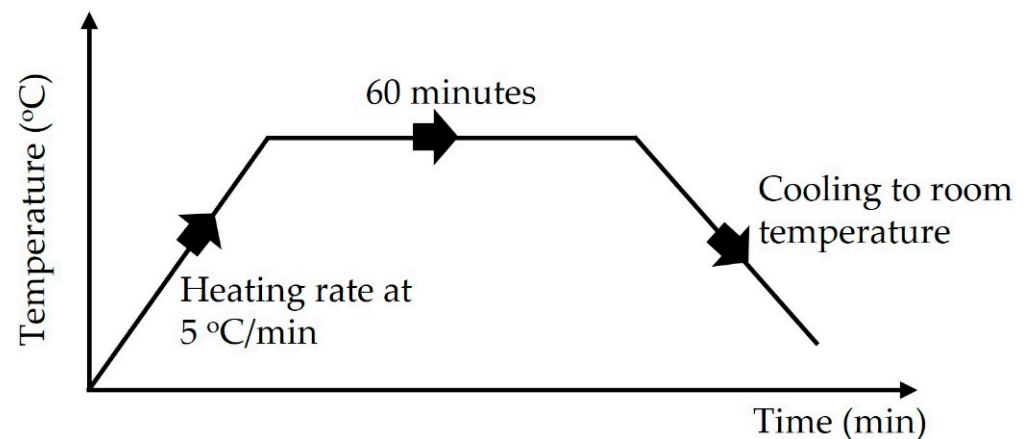


Figure 3. The calcination process of the geopolymer mortar.

2.3. High-Temperature Exposure Impact on Compressive Strength

A digital compressive testing equipment with a capacity of 3000 kN was used in this work to measure the strength of geopolymer mortar specimens using a standard test technique (ASTM C109/C109 M standard) [35] after temperature exposure. The three cubes were subjected to forces at a rate of 0.9 kN/s until the mortar samples failed in each compressive strength test. It was determined what the average compressive strength was. The load was divided by a cross-sectional area to determine the strength.

2.4. Characterization Studies

Some parts of the crushed cubes after the compressive strength test were gathered, milled, and sieved through a No. 200 mesh for the characterization studies. The crack surface characteristics of the specimens were investigated using FESEM. The micrograph images of the geopolymer mortar were captured using Carl Zeiss's ultra-high-resolution SUPRA 66VP. FTIR spectrum was used to evaluate the absorption of particles and transmission producing a molecular impression of geopolymer mortar samples. The scans were done from 400 cm⁻¹ to 4000 cm⁻¹ wave-number, at 100 cycles and 4 cm⁻¹ resolutions to record the spectrum. The samples were analyzed using a Varian 3100 FTIR coupled with Varian 600 UMA FTIR. To study mineral composition and crystalline patterns for the exposed mortar samples, XRD test was carried out using Bruker's X-ray diffraction instrument. The mortar samples were scanned from 0° to 80° 2θ at laboratory temperature using a Cu Kα radiation with 0.0262 scan step size. The pattern intensities were observed using a constant divergence slit of 0.38 mm along with Cu as the anode material by using two reflection coefficients Ka1 of 1.5406 and Ka2 of 1.5444. The identification of minerals was carried out using an X'pert high score plus package software.

The distributions and sizes of pores in geopolymer mortar were studied using MIP. The test was carried out in accordance with ASTM D4284 standard procedures. Thermo-fisher scientific porosimeter was connected to a computer data collecting system with software to obtain pore measurements from the Porosimeter. Crushing the cubes of geopolymer

mortar was used to treat the samples (about 10 mm). The samples were preconditioned before the test to remove any contamination from the pore walls and pores. Out-gassing the samples for around 8 h at 105 °C in a lower pressure vacuum of about 1.3 Pa was used to accomplish this. The weights of outgassed samples were measured. The outgassed specimens were placed in the penetrometer. The penetrometer was then placed in an appropriate chamber and displaced to a pressure of 1.3 Pa. The penetrometer was loaded up with mercury by putting relatively small pressure. The filled penetrometer was then placed in the porosimeter's pressure flask and prepared for measurements of pressure and penetration. The pressure was consistently increased, and the interrupted absolute pressure of mercury and volume were reported by the data capturing system until optimum pressure was reached. The pressure was decreased after finishing the pressure cycle and the equipment was dismantled and thoroughly washed. The results were retrieved from the system of data acquisition. A blank test (an intrusion test) on a non-permeable specimen was then conducted to get compressibility values and temperature changes to be utilized to address intrusion data. The non-porous specimen was examined in a similar way to that of geopolymer mortar samples. The results of the blank test were used to adjust the intruded volume by either including or deducting the values from the volumes of intrusion.

3. Results, Analysis, and Discussion

In this study, fly ash-based geopolymer mortar formulation having petroleum sludge ash as a substitute precursor material was exposed to different temperatures (200 °C, 400 °C, 600 °C, 800 °C, and 1000 °C). The obtained results, from the various tests, conducted, are discussed in the following sections.

3.1. Residual Compressive Strength after Temperature Exposures

Figure 4 depicts the residual compressive strength of the blend of fly ash and petroleum sludge ash after exposure to different temperatures. After an oven curing at 60 °C, the compressive strength of the geopolymer mortar, the reference value, is 31.58 MPa which is higher than the compressive strength of mortars exposed to higher temperatures. The compressive strength of the control geopolymer is mainly associated with sodium aluminosilicate hydrate (N-A-S-H) gel as identified in the FESEM investigation. As the temperature increased (200 °C, 400 °C, 600 °C, 800 °C, and 1000 °C.), the compressive strength of mortar samples decreased by 19.57%, 42.78%, 53.29%, 64.28%, and 72.73%, respectively. This is attributed to the transportation of the chemically and physically bonded water, the transformation of geopolymer mortar phases, OH groups, anhydrous products development, and the sintering process. From a temperature of 400 °C and above, the strength decreased due to the thermal stress that initiated cracks on the geopolymer mortar samples. Beyond 600 °C, the amorphousness of the geopolymer matrix started to change to a crystalline structure and a similar result was reported by [36]. A comparable trend of the new crystalline structure formation at higher temperatures was found in the XRD investigation of this study. At higher temperatures, non-uniform recrystallization occurs, resulting in the formation of big cracks which therefore decrease strength [4].

3.2. Analysis of Mercury Intrusion Porosimetry

The MIP test was used to assess the porosity of geopolymer mortar samples after exposure to various temperatures. The results of cumulative porosity of the geopolymer mortars as pore diameter functions are shown in Figure 5. The temperature effect on the geopolymer mortar soundness may be evaluated in terms of the increased or decreased distribution of pore diameter, the total volume of pores, and accessible porosity. From Figure 5, the cumulative pore volume of geopolymer mortars exposed to 60 °C, 200 °C, 400 °C, 600 °C, 800 °C, and 1000 °C (GPM-60 °C, GPM-200 °C, GPM-400 °C, GPM-600 °C, GPM-800 °C, and GPM-1000 °C) are 24.52 mm³/g, 31.14 mm³/g, 98.31 mm³/g, 106.16 mm³/g, 156.41 mm³/g, and 114 mm³/g, respectively. It was observed that with the increase in temperature, the cumulative pore volume increased. The lower porosity of the reference geopolymer mortar

subjected to a temperature of 60 °C (GPM-60 °C) results in higher compressive strength. The porosity value, in this study, at the final temperature (1000 °C) was higher than the control value by more than a factor of two. The porosity increase in the geopolymer mortar is associated with cracking and had a destructive effect on the structure of the material and damage evolution [37]. Table 3 also includes some interesting index parameters that define the properties of a penetrable structure. The volume change of the mercury penetration was used to determine the average pore diameter, median pore diameter, and total surface area of the pores [38]. The modal pore diameter was determined by the fluctuation in pore volume as a function of strength variation. The average pore diameter ranged between 74.34 and 11,895.25 nm, as shown in the table.

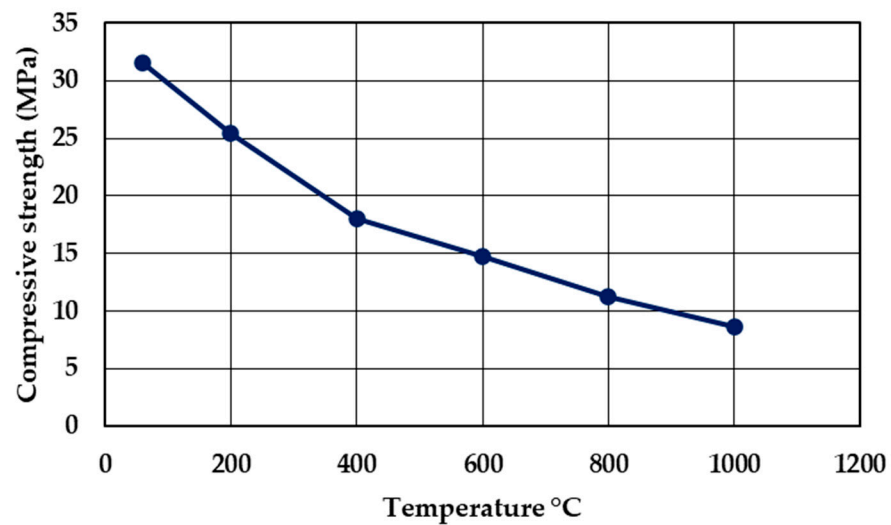


Figure 4. Residual compressive strength at different temperatures.

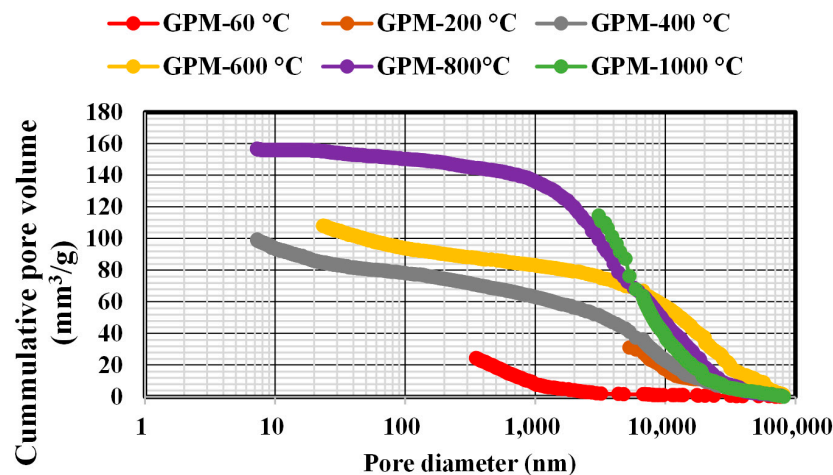


Figure 5. Pore size distribution for geopolymer mortar containing.

Table 3. Pore structure properties of geopolymer mortar.

Temp. (°C)	Modal Pore Diameter D10 (nm)	Median Pore Diameter D90 (nm)	Average Pore Diameter D50 (nm)	Apparent Density (g/cm ³)	Total Surface Area (m ² /g)	Porosity (%)
60	11.44	325.17	74.34	9.82	2.75	33.39
200	11,939.32	10,854.58	11,895.25	2.03	0.01	3.90
400	7.29	5272.90	87.98	2.85	3.76	19.08
600	20,046.41	10,741.60	173.04	3.10	2.56	25.54
800	18,500.70	4598.22	498.58	3.21	1.24	33.10
1000	6740.01	7735.72	6905.72	2.21	0.04	12.77

3.3. Fourier-Transform Infrared Spectroscopy

Figure 6 depicts the FTIR spectra of the specimens after exposure to different elevated temperatures. The reference sample (GPM-60 °C) had a broad absorption band, around 1009.72 cm^{-1} , caused by the asymmetric bending vibration of Si-O-Al and Si-O-Si (Si-O-T). This peak shifted to the right and increased by a small amount after the exposure of samples to higher temperatures, which is a key indicator of geopolymerization. This shift indicates that the number of Si-O-T bonds increased because of the dihydroxylation process [39]. During the geopolymerization reaction, Al atoms were inserted into the network of geopolymer which increase the amount of non-bridged oxygen atoms. Si-O-T peak comprises a series of peaks that partly overlap with one another. The absorption peak around 3435 cm^{-1} corresponds to the stretching vibrations of the Si-OH bond OH group (hydroxyl). The peak adsorbed water molecules on the precursor surface. The assigned absorption peaks to the bending vibration of the -OH and H-O-H group of the hydrated products of reaction that are related to water appear at 1650 cm^{-1} . From 690 to 780 cm^{-1} , absorption bands are designated to Si-O-Si and Al-O-Si vibrations which are attributed to the formation of N-A-S-H. Around 777 cm^{-1} , the absorption peak indicated the existence of quartz (Si-O) functional groups.

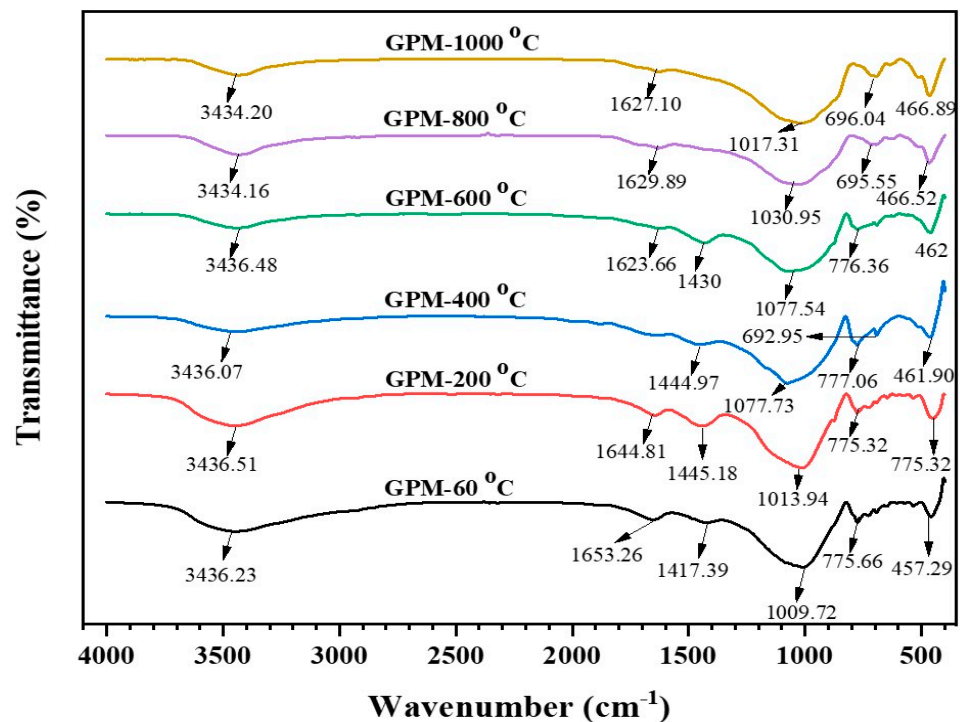


Figure 6. FTIR spectra of the geopolymer mortar after exposure to high temperatures.

3.4. X-ray Diffraction (XRD) Analysis

XRD was conducted to examine the nature and composition of the reaction products in geopolymer mixtures. Figure 7 depicts the XRD patterns of the specimens after exposure to different elevated temperatures (60 °C, 200 °C, 400 °C, 600 °C, 800 °C, and 1000 °C). The patterns display a noisy and broad background between 20° and 60° 2-theta and the amorphous gels formation of the geopolymerization can be confirmed from the broad humps. Similar findings were reported by [40]. The thermally stable quartz which is present in the fly ash was found at all temperatures [41]. The XRD evaluation revealed that carbon begins to form at 800 °C. Sodium silicate and aluminum were seen at 1000 °C. Quartz is widely seen in this temperature range in FA-based geopolymer mortars. The uneven transformation of phases at elevated temperatures results in the geopolymer matrix breakdown, volume expansion, as well as changes in the microstructure. The volume

difference in the geopolymer matrix results in high stress on the material and speeds up crack formation [42]. This high stress and crack formation led to the loss in compressive strength at temperatures over 800 °C.

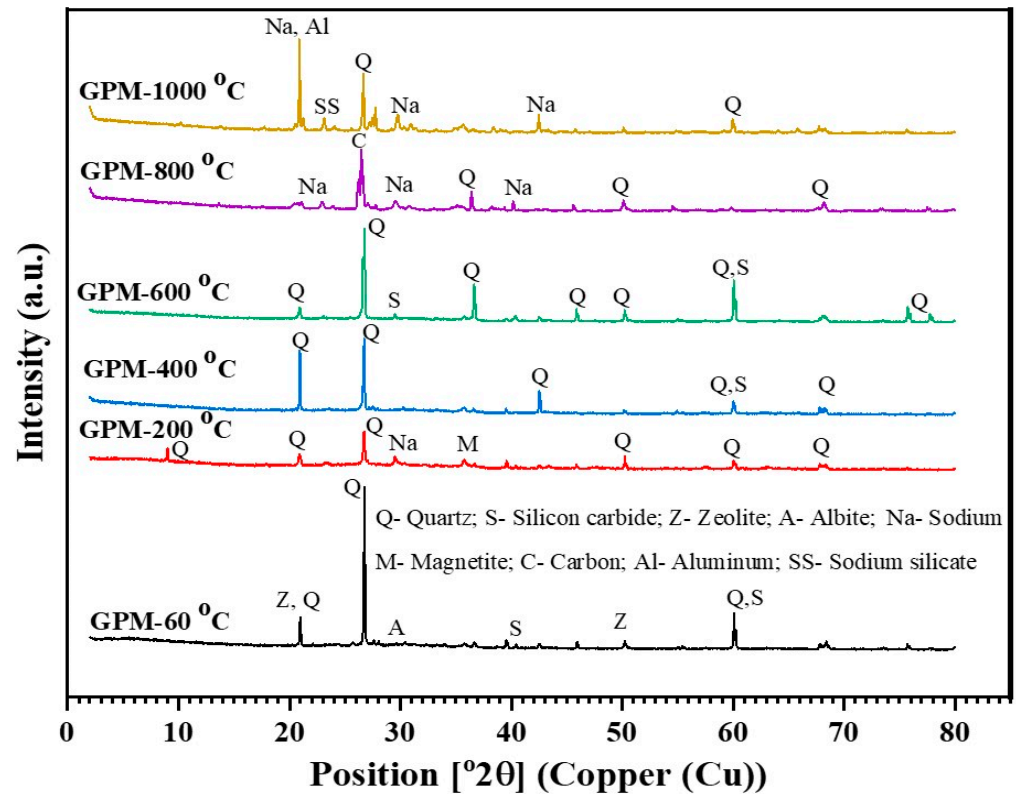


Figure 7. X-ray diffraction spectra of geopolymer mortar subjected to various temperatures.

3.5. Field Emission Scanning Electron Microscope (FESEM) Analysis

Figure 8 depicts the images of the microstructure of calcined geopolymer mortars and shows noticeable changes in the microstructure of the geopolymer matrices as heated to 1000 °C. For the amorphous structure of the geopolymer mortar sample heated at 60 °C, it shows unreacted fly ash particles, reaction products, voids, and cracks observed in Figure 8A. When the heating temperature increased to 200 °C (Figure 8B), a smaller amount of partly reacted fly ash particles were observed, and more reaction products were seen. At a temperature of 400 °C (Figure 8C), a small number of new products was seen around partly-reacted particles of fly ash. This finding is in line with reported results [43]. The microstructure of geopolymer mortar after exposure to temperatures of 600 °C is shown in Figure 8D. The matrix shows no new reaction products. At this temperature, decomposition of the geopolymer matrix begins with porosity increasing. Figure 8E,F depict the geopolymer mortars exposed to temperatures of 800 °C and 1000 °C. The matrices are similar to interconnected pores which decreased the compressive strength of the geopolymer [44]. Significantly fewer partly-reacted fly ash particles and visible cracks in the microstructure were noticed. This was because of the higher pressure that elevated temperature applied in the matrices of geopolymer mortars [23]. At the temperature of 1000 °C, the micrograph showed a large void that was approximately 2–10 μm in diameter. This porosity was due to materials decomposition after calcination [45]. EDX quantitative determination of the main geopolymer mortar elements before and after exposure to different high temperatures is shown in Figure 9.

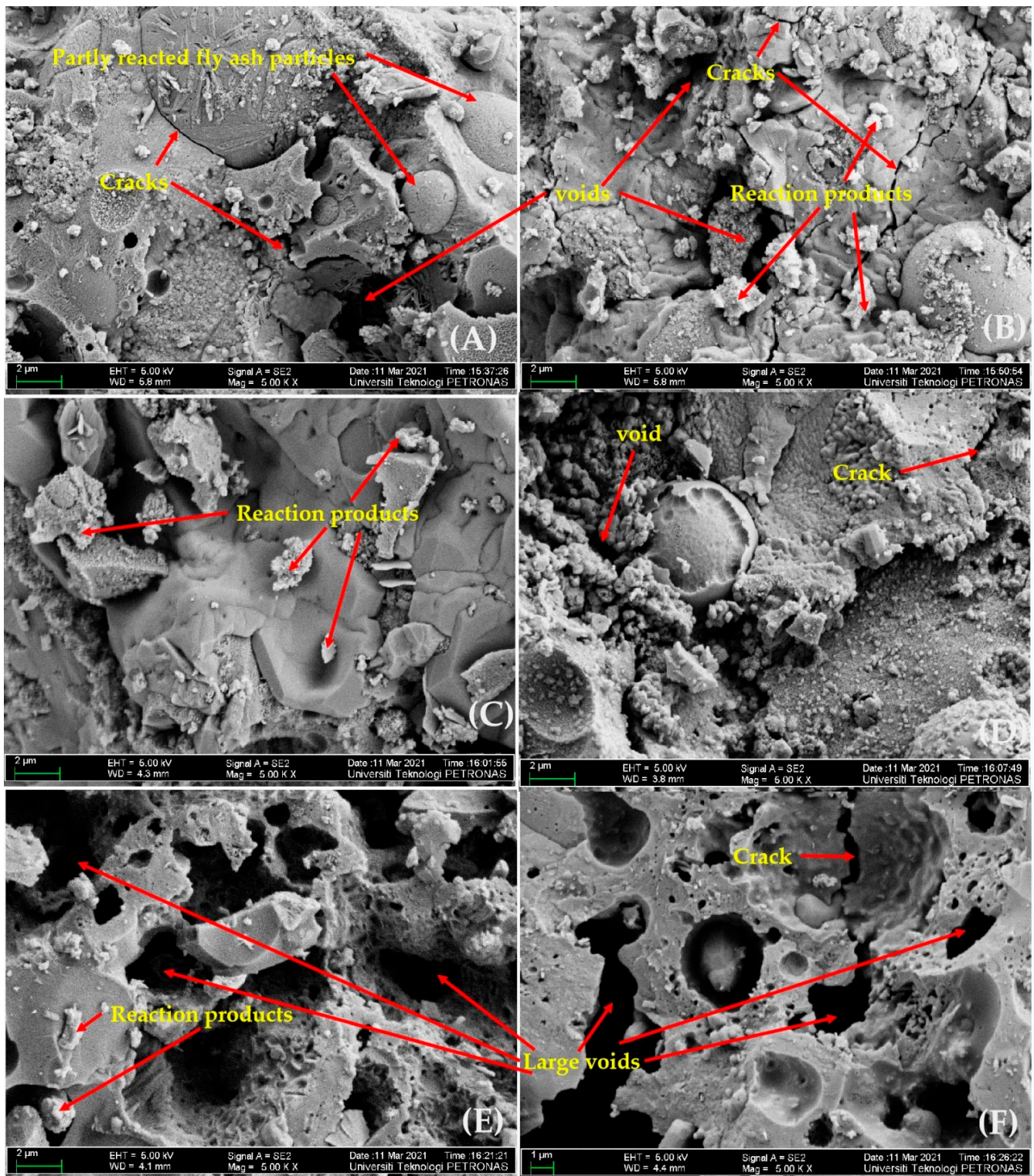


Figure 8. Morphology of geopolymer mortars at temperatures of (A) 60 °C, (B) 200 °C, (C) 400 °C, (D) 600 °C, (E) 800 °C, and (F) 1000 °C.

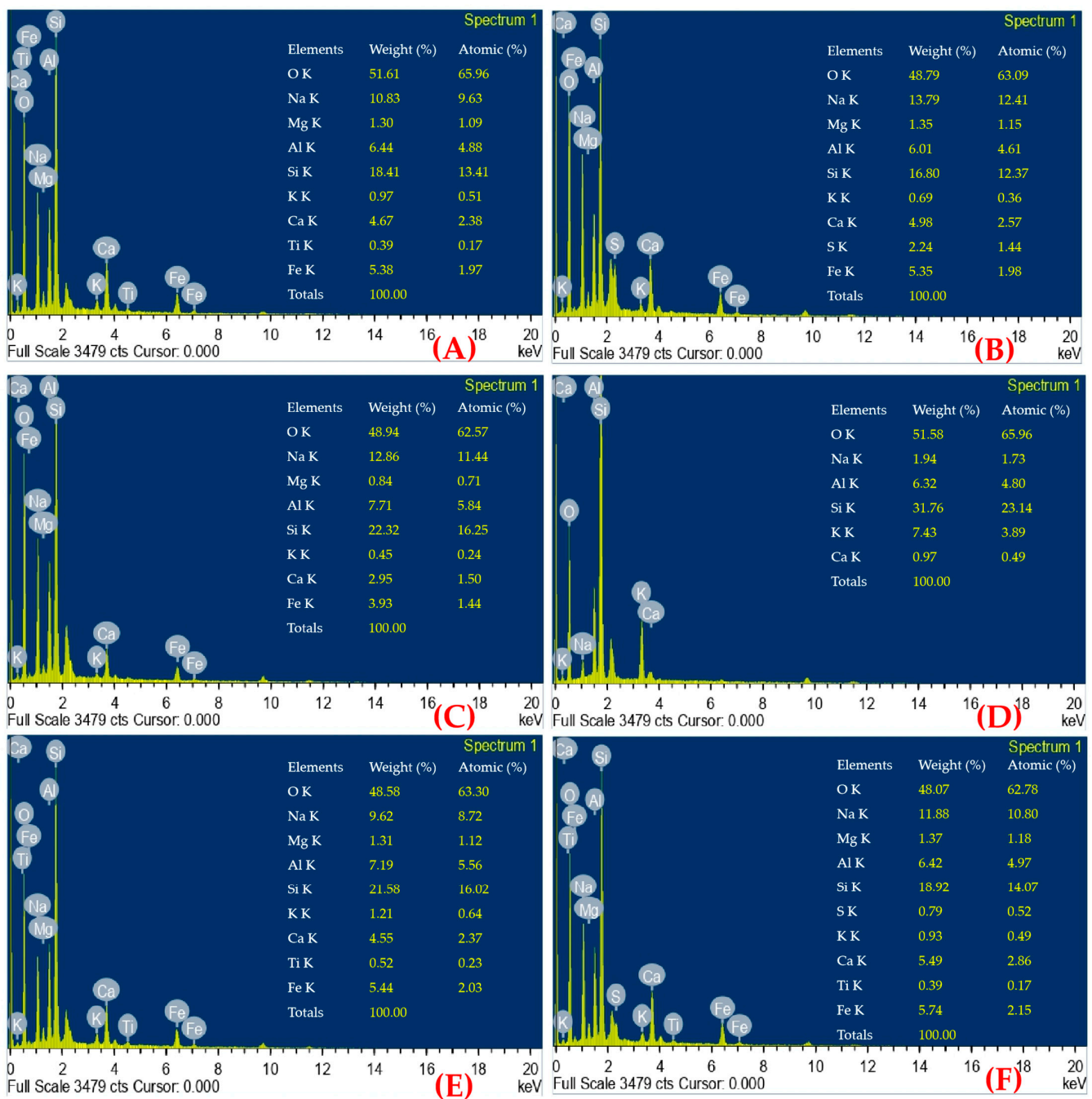


Figure 9. EDX quantitative determination of the geopolymer mortar elements at temperatures of (A) 60 °C, (B) 200 °C, (C) 400 °C, (D) 600 °C, (E) 800 °C, and (F) 1000 °C.

4. Conclusions

Based on the experimental findings of this study, the following conclusions were made:

1. After an oven curing at 60 °C, the compressive strength of the geopolymer mortar, the reference value, is 31.58 MPa which is higher than the compressive strength of mortars exposed to higher temperatures. As the temperature increased (200 °C, 400 °C, 600 °C, 800 °C, and 1000 °C.), the compressive strength of mortar samples decreased by 19.57%, 42.78%, 53.29%, 64.28%, and 72.73% respectively.
2. Up to 200 °C, the geopolymer mortar can sustain significant compressive strength after temperature exposure.

3. The cumulative pore volume of geopolymer mortars exposed to 60 °C, 200 °C, 400 °C, 600 °C, 800 °C, and 1000 °C are 24.52 mm³/g, 31.14 mm³/g, 98.31 mm³/g, 106.16 mm³/g, 156.41 mm³/g, and 114 mm³/g respectively. It was observed that with the increase in temperature, the cumulative pore volume increased.
4. The FTIR spectra of the specimens after exposure to different elevated temperatures depicted broad absorption bands, which are the key indicator of geopolymerization reaction. The XRD patterns display a noisy and broad background between 20° and 60° 2-theta and the amorphous gels formation of the geopolymerization can be confirmed from the broad humps.
5. The FESEM image of the geopolymer mortar sample cured at 60 °C, showed unreacted fly ash particles, reaction products, voids, and cracks. At a temperature of 600 °C, decomposition of the geopolymer matrix begins with porosity increasing. The geopolymer mortar is exposed to the temperature of 800 °C and 1000 °C, the matrices are similar to interconnected pores which decreased the compressive strength of the geopolymer because of the higher pressure that elevated temperature exerted in the matrices of geopolymer mortars.

Author Contributions: Conceptualization, M.U.K. and L.B.; methodology, M.U.K. and N.D.; validation M.U.K., L.B., N.D., A.B. and S.I.M.; investigation, M.U.K.; resources, L.B.; data curation, L.B.; writing—original draft preparation, M.U.K.; writing—review and editing, M.U.K., N.D., A.B. and S.I.M.; visualization, M.U.K. and N.D.; supervision, L.B.; funding acquisition, L.B. and N.A.Z. All authors have read and agreed to the published version of the manuscript.

Funding: The authors thank UTP for supporting the research under the YUTP grant (015LC0-303).

Institutional Review Board Statement: Not applicable.

Informed Consent Statement: Not applicable.

Data Availability Statement: Not applicable.

Acknowledgments: The authors are also thankful to Johan Ariff B. Mohamed, Zaaba bin Mohammad, Meor Asniwan Bin Mew Ghazali, from the Department of Civil and Environmental Engineering, Universiti Teknologi PETRONAS, Malaysia for their assistance. Ir. Fazli Rahim for providing the contact to obtain the sludge.

Conflicts of Interest: The authors declare no conflict of interest.

References

1. Drzymała, T.; Jackiewicz-Rek, W.; Gałąż, J.; Śukys, R. Assessment of mechanical properties of high strength concrete (HSC) after exposure to high temperature. *J. Civ. Eng. Manag.* **2018**, *24*, 138–144. [[CrossRef](#)]
2. Rudnik, E.; Drzymała, T. Thermal behavior of polypropylene fiber-reinforced concrete at elevated temperatures. *J. Therm. Anal.* **2018**, *131*, 1005–1015. [[CrossRef](#)]
3. Jackiewicz-Rek, W.; Drzymała, T.; Kuś, A.; Tomaszewski, M. Durability of High Performance Concrete (HPC) Subject to Fire Temperature Impact. *Arch. Civ. Eng.* **2016**, *62*, 73–94. [[CrossRef](#)]
4. Luhar, S.; Chaudhary, S.; Luhar, I. Thermal resistance of fly ash based rubberized geopolymer concrete. *J. Build. Eng.* **2018**, *19*, 420–428. [[CrossRef](#)]
5. Handoo, S.; Agarwal, S. Physicochemical, mineralogical, and morphological characteristics of concrete exposed to elevated temperatures. *Cem. Concr. Res.* **2002**, *32*, 1009–1018. [[CrossRef](#)]
6. Hager, I.; Sitarz, M.; Mróz, K. Fly-ash based geopolymer mortar for high-temperature application—Effect of slag addition. *J. Clean. Prod.* **2021**, *316*, 128168. [[CrossRef](#)]
7. Abadel, A.A.; Albidah, A.S.; Altheeb, A.H.; Alrshoudi, F.A.; Abbas, H.; Al-Salloum, Y.A. Effect of molar ratios on strength, microstructure & embodied energy of metakaolin geopolymer. *J. Adv. Concr. Constr* **2021**, *11*, 127–140.
8. Khoury, G.A. Compressive strength of concrete at high temperatures: A reassessment. *Mag. Concr. Res.* **1992**, *44*, 291–309. [[CrossRef](#)]
9. Arioz, O. Retained properties of concrete exposed to high temperatures: Size effect. *Fire Mater.* **2009**, *33*, 211–222. [[CrossRef](#)]
10. Jagaba, A.; Kutty, S.; Hayder, G.; Baloo, L.; Noor, A.; Yaro, N.; Saeed, A.; Lawal, I.; Birniwa, A.; Usman, A. A Systematic Literature Review on Waste-to-Resource Potential of Palm Oil Clinker for Sustainable Engineering and Environmental Applications. *Materials* **2021**, *14*, 4456. [[CrossRef](#)]

11. Ghaleb, A.A.S.; Kutty, S.R.M.; Ho, Y.-C.; Jagaba, A.H.; Noor, A.; Al-Sabaei, A.M.; Almahbashi, N.M.Y. Response Surface Methodology to Optimize Methane Production from Mesophilic Anaerobic Co-Digestion of Oily-Biological Sludge and Sugarcane Bagasse. *Sustainability* **2020**, *12*, 2116. [CrossRef]
12. Jagaba, A.H.; Shuaibu, A.; Umaru, I.; Musa, S.; Lawal, I.M.; Abubakar, S. Stabilization of soft soil by incinerated sewage sludge ash from municipal wastewater treatment plant for engineering construction. *Sustain. Struct. Mater* **2019**, *2*, 32–44.
13. Kankia, M.U.; Baloo, L.; Danlami, N.; Samahani, W.N.; Mohammed, B.S.; Haruna, S.; Jagaba, A.H.; Abubakar, M.; Ishak, E.A.; Sayed, K.; et al. Optimization of Cement-Based Mortar Containing Oily Sludge Ash by Response Surface Methodology. *Materials* **2021**, *14*, 6308. [CrossRef] [PubMed]
14. Zhang, Z.; Provis, J.L.; Reid, A.; Wang, H. Geopolymer foam concrete: An emerging material for sustainable construction. *Constr. Build. Mater.* **2014**, *56*, 113–127. [CrossRef]
15. Yaro, N.; Napiah, M.; Sutanto, M.; Usman, A.; Jagaba, A.; Mani, A.; Ahmad, A. *Geopolymer Utilization in the Pavement Industry-An Overview*; IOP Conference Series: Earth and Environmental Science; IOP Publishing: Bristol, UK, 2022; p. 012025.
16. Qu, F.; Li, W.; Tao, Z.; Castel, A.; Wang, K. High temperature resistance of fly ash/GGBFS-based geopolymer mortar with load-induced damage. *Mater. Struct.* **2020**, *53*, 111. [CrossRef]
17. Albidah, A.; Abadel, A.; Alrshoudi, F.; Altheeb, A.; Abbas, H.; Al-Salloum, Y. Bond strength between concrete substrate and metakaolin geopolymer repair mortars at ambient and elevated temperatures. *J. Mater. Res. Technol.* **2020**, *9*, 10732–10745. [CrossRef]
18. Kim, Y.; Kim, K.; Jeong, G.-Y. Study of detailed geochemistry of hazardous elements in weathered coal ashes. *Fuel* **2017**, *193*, 343–350. [CrossRef]
19. Dao, D.V.; Forth, J.P. Investigation of the behaviour of geopolymer mortar after heating to elevated temperatures. In Proceedings of the Third International Conference on Sustainable Construction Materials and Technologies, Kyoto, Japan, 18–21 August 2013.
20. Turkey, F.A.; Beddu, S.B.; Ahmed, A.N.; Al-Hubboubi, S. A review—Behaviour of geopolymer concrete to high temperature. *Mater. Today Proc.* **2021**. [CrossRef]
21. Chithambaram, S.J.; Kumar, S.; Prasad, M. Thermo-mechanical characteristics of geopolymer mortar. *Constr. Build. Mater.* **2019**, *213*, 100–108. [CrossRef]
22. Lawal, I.M.; Bertram, D.; White, C.J.; Jagaba, A.H.; Hassan, I.; Shuaibu, A. Multi-Criteria Performance Evaluation of Gridded Precipitation and Temperature Products in Data-Sparse Regions. *Atmosphere* **2021**, *12*, 1597. [CrossRef]
23. Zhang, H.Y.; Kodur, V.; Wu, B.; Cao, L.; Wang, F. Thermal behavior and mechanical properties of geopolymer mortar after exposure to elevated temperatures. *Constr. Build. Mater.* **2016**, *109*, 17–24. [CrossRef]
24. Ranjbar, N.; Mehrali, M.; Alengaram, U.J.; Metselaar, H.S.C.; Jumaat, M.Z. Compressive strength and microstructural analysis of fly ash/palm oil fuel ash based geopolymer mortar under elevated temperatures. *Constr. Build. Mater.* **2014**, *65*, 114–121. [CrossRef]
25. Chi, M.; Huang, R. Binding mechanism and properties of alkali-activated fly ash/slag mortars. *Constr. Build. Mater.* **2013**, *40*, 291–298. [CrossRef]
26. Guerrieri, M.; Sanjayan, J.G. Behavior of combined fly ash/slag-based geopolymers when exposed to high temperatures. *Fire Mater.* **2009**, *34*, 163–175. [CrossRef]
27. Ismail, I.; Bernal, A.S.; Provis, J.L.; Hamdan, S.; Van Deventer, J.S.J. Microstructural changes in alkali activated fly ash/slag geopolymers with sulfate exposure. *Mater. Struct.* **2012**, *46*, 361–373. [CrossRef]
28. Kankia, M.U.; Baloo, L.; Danlami, N.; Mohammed, B.S.; Haruna, S.; Abubakar, M.; Jagaba, A.H.; Sayed, K.; Abdulkadir, I.; Salihi, I.U. Performance of Fly Ash-Based Inorganic Polymer Mortar with Petroleum Sludge Ash. *Polymers* **2021**, *13*, 4143. [CrossRef]
29. *ACTM C 618-03*; Standard Specification for Coal Fly Ash and Raw or Calcined Natural Pozzolan for Use in Concrete. ASTM International: West Conshohocken, PA, USA, 2003. [CrossRef]
30. Ghaleb, A.; Kutty, S.; Salih, G.; Jagaba, A.; Noor, A.; Kumar, V.; Almahbashi, N.; Saeed, A.; Al-Dhawi, B.S. Sugarcane Bagasse as a Co-Substrate with Oil-Refinery Biological Sludge for Biogas Production Using Batch Mesophilic Anaerobic Co-Digestion Technology: Effect of Carbon/Nitrogen Ratio. *Water* **2021**, *13*, 590. [CrossRef]
31. C09 Committee Specification for Concrete Aggregates. 2013. Available online: https://www.astm.org/c0033_c0033m-13.html (accessed on 5 February 2022). [CrossRef]
32. Payakaniti, P.; Chuewangkam, N.; Yensano, R.; Pinitsoontorn, S.; Chindaprasirt, P. Changes in compressive strength, microstructure and magnetic properties of a high-calcium fly ash geopolymer subjected to high temperatures. *Constr. Build. Mater.* **2020**, *265*, 120650. [CrossRef]
33. Jagaba, A.H.; Kutty, S.R.M.; Lawal, I.M.; Aminu, N.; Noor, A.; Al-Dhawi, B.N.S.; Usman, A.K.; Batari, A.; Abubakar, S.; Birniwa, A.H.; et al. Diverse sustainable materials for the treatment of petroleum sludge and remediation of contaminated sites: A review. *Clean. Waste Syst.* **2022**, *2*, 100010. [CrossRef]
34. Kankia, M.U.; Baloo, L.; Mohammed, B.S.; Hassan, S.B.; Haruna, S.; Danlami, N.; Ishak, E.A.; Samahani, W.N. Effects of petroleum sludge ash in fly ash-based geopolymer mortar. *Constr. Build. Mater.* **2020**, *272*, 121939. [CrossRef]
35. Bakharev, T.; Sanjayan, J.; Cheng, Y.-B. Alkali activation of Australian slag cements. *Cem. Concr. Res.* **1999**, *29*, 113–120. [CrossRef]
36. Karakoç, M.B.; Türkmen, I.; Maraş, M.M.; Kantarci, F.; Demirboğa, R.; Toprak, M.U. Mechanical properties and setting time of ferrochrome slag based geopolymer paste and mortar. *Constr. Build. Mater.* **2014**, *72*, 283–292. [CrossRef]

37. ASTM C109/109M; Standard Test Method for Compressive Strength of Hydraulic Cement Mortars (Using 2-in. or [50-mm] Cube Specimens). ASTM International: West Conshohocken, PA, USA, 2013.
38. Ghaleb, A.; Kutty, S.; Ho, Y.; Jagaba, A.; Noor, A.; Al-Sabaei, A.; Kumar, V.; Saeed, A. *Anaerobic Co-Digestion for Oily-Biological Sludge with Sugarcane Bagasse for Biogas Production under Mesophilic Condition*; IOP Conference Series: Materials Science and Engineering; IOP Publishing: Bristol, UK, 2020; p. 012084.
39. Yang, Z.; Mocadlo, R.; Zhao, M.; Sisson, R.D.; Tao, M.; Liang, J. Preparation of a geopolymer from red mud slurry and class F fly ash and its behavior at elevated temperatures. *Constr. Build. Mater.* **2019**, *221*, 308–317. [[CrossRef](#)]
40. Behera, P.; Baheti, V.; Militky, J.; Louda, P. Elevated temperature properties of basalt microfibril filled geopolymer composites. *Constr. Build. Mater.* **2017**, *163*, 850–860. [[CrossRef](#)]
41. Martin, A.; Pastor, J.Y.; Palomo, A.; Jiménez, A.F. Mechanical behaviour at high temperature of alkali-activated alumi-nosilicates (geopolymers). *Constr. Build. Mater.* **2015**, *93*, 1188–1196. [[CrossRef](#)]
42. Torres-Carrasco, M.; Puertas, F. Waste glass in the geopolymer preparation: Mechanical and microstructural characterisation. *J. Clean. Prod.* **2015**, *90*, 397–408. [[CrossRef](#)]
43. Jiang, X.; Xiao, R.; Zhang, M.; Hu, W.; Bai, Y.; Huang, B. A laboratory investigation of steel to fly ash-based geopolymer paste bonding behavior after exposure to elevated temperatures. *Constr. Build. Mater.* **2020**, *254*, 119267. [[CrossRef](#)]
44. Sarker, P.K.; Kelly, S.; Yao, Z. Effect of fire exposure on cracking, spalling and residual strength of fly ash geopolymer concrete. *Mater. Des.* **2014**, *63*, 584–592. [[CrossRef](#)]
45. Abdullah, M.M.A.B.; Jamaludin, L.; Hussin, K.; Bnhussain, M.; Ghazali, C.M.R.; Ahmad, M.I. Fly Ash Porous Material using Geopolymerization Process for High Temperature Exposure. *Int. J. Mol. Sci.* **2012**, *13*, 4388–4395. [[CrossRef](#)] [[PubMed](#)]

Disclaimer/Publisher’s Note: The statements, opinions and data contained in all publications are solely those of the individual author(s) and contributor(s) and not of MDPI and/or the editor(s). MDPI and/or the editor(s) disclaim responsibility for any injury to people or property resulting from any ideas, methods, instructions or products referred to in the content.